Annals of Nanoscience and Nanotechnology

Original Research
Published: 30 Nov, 2017

Optoelectronic Ultrafast Tunability in VO_2 Based Mott/ Peierls Nanostructures

M. Maaza[1,2]*

[1]UNESCO-UNISA Africa Chair in Nanosciences/Nanotechnology, College of Graduate Studies, University of South Africa, Pretoria-South Africa

[2]Nanosciences African Network (NANOAFNET), iThemba LABS-National Research Foundation, Somerset West, Western Cape Province, South Africa

Abstract

Being a Mott/Peierls type oxide, at a temperature of about 68°C and ambient pressure, stoichiometric VO_2 undergoes a first order metal-insulator transition, which is accompanied by a femtosecond structural transition from a high-temperature rutile to a low-temperature monoclinic phase. This reversible phenomenon causes an abrupt and significant change in the resistivity over several orders of magnitude induced by the band gap opening/closure. From optical point of view, this metal-semiconductor transition is accompanied by a significant and reversible variation of the refractive index under thermal stimuli in the infrared spectral range. Hence, VO_2 based coatings have been attracting considerable interest for fundamental reasons, and certainly for technological applications in the solar energy sector and ultrafast linear and nonlinear photonics as well as opto-electronics. In this contribution, specific opto-electronic multi-functionality of nanostructured VO_2 based coatings is presented. This includes applications such as (i) Active coating for solar heat management in buildings and automotives as a smart window, (ii) Tunable emissivity based coatings for satellites applications, (iii) Ultrafast opto-electronic gating, (iv) Optical limiting, (v) Femtosecond tunable nano-plasmonics in addition to room temperature H_2 gas sensing.

Keywords: Vanadium dioxide; Phase transition, Refractive index modulation; NIR; Plasmon tenability; Smart Windows; Nano-plasmonics; Ultrafast transition

OPEN ACCESS

Correspondence:
Maaza M, Nanosciences African Network (NANOAFNET), iThemba LABS-National Research Foundation, 1 Old Faure road, Somerset West 7129, POBox 722, Somerset West, Western Cape Province, South Africa, Tel: +27218431145; E-mail: Maaza@tlabs.ac.za

Received Date: *04 Aug 2017*
Accepted Date: *15 Nov 2017*
Published Date: *30 Nov 2017*

Citation:
M. Maaza. Optoelectronic Ultrafast Tunability in VO_2 Based Mott/ Peierls Nanostructures. Ann Nanosci Nanotechnol. 2017; 1(1): 1002.

Introduction

Within the smart materials family, there is a significant population of oxides at the nanoscale which are extensively investigated for their promising technological as well as from fundamental viewpoint. Figure 1 report some of the most studied ones in relation to their tunable physical properties. Among such oxides, one can single out metal-insulator (MIT) or metal-semiconductor (MIS) phase transition oxides family. More accurately and in such a category, Vanadium dioxide VO_2 is of a special interest both fundamentally and technologically as its transition T_c is close to room temperature (~68°C) and hence its potential multifunctional application in optoelectronics.

From crystallographic view point, in the late 50s up to the 70s [1-11], it was established that the V-O system crystallizes in a variety of stable oxides in accordance to its rich electronic valence (from 0 to +5) including Magnussen (V_nO_{2n-1}) as well as Wadsley ($V_{2n}O_{5n-2}$) type structures as summarized in Figure 2. As highlighted above, the specific +4 valence of vanadium oxide i.e. VO_2 which is stable in a limited region of the V-O phase diagram is of a special interest. While it took nearly a half-century since the pioneering works of Morin and Sir Neville Mott to measure the duration of the singular 1st order metal-insulator transition (MIT) of VO_2 which was found to be in the femtosecond regime by Cavalleri et al [7], VO_2 is gaining an exponential interest within the R&D community [12-24]. Being a smart oxide, transiting reversibly at T_c~ 341K, stoichiometric VO_2 undergoes a unique 1st order metal-semiconductor electronic transition with a reversible opening-closing of its band gap from 0.72 to 0 eV (Figure 3). Such a reversible semiconductor-metallic phase transition is also accompanied by a large variation of the electrical resistance/conductivity by several orders of magnitude being in the bulk or in its thin film configuration (Figure 4 and Table 1). This tunability of the electronic band gap and hence the electrical resistance/conductivity are correlated to a reversible crystallographic 1st order transition [25-27]; from low temperature monoclinic to high temperature tetragonal and vice-versa. More accurately, above T_c, VO_2 crystallizes in a tetragonal rutile-type with lattice constants of a~ 0.455 nm and c~ 0.285 nm. The second is the monoclinic

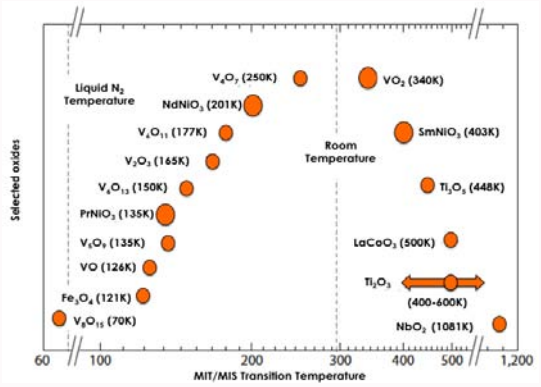

Figure 1: Major oxides exhibiting semiconductor-metal or/and insulator-metal phase transitions.

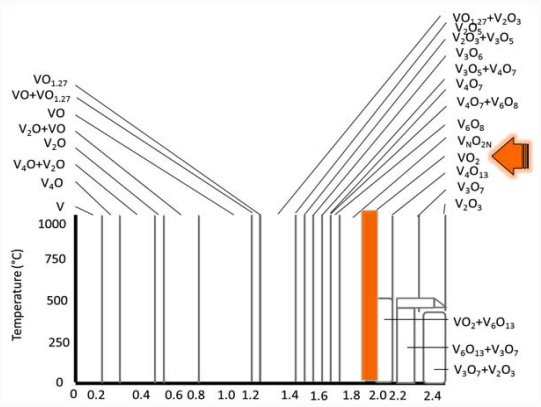

Figure 2: Basic phase diagram of V-O system rich in Magnussen (VnO_2n-1) and Wadsley (V_2NO_5n-2) type structures.

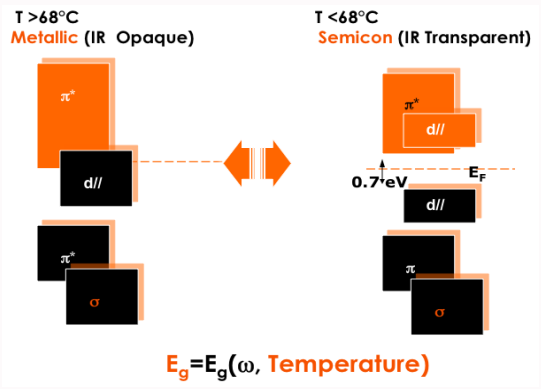

Figure 3: Tunable & reversible opening/closing of VO_2 bangap Eg (T) via the splitting of the d band.

VO_2 with a~ 0.5753 nm, b~ 0.4526 nm and c~ 0.5383 nm. A third monoclinic VO_2 structure does exist too, but with a~ 1.209 nm, b~ 0.3702 nm and c~ 0.6433 nm. However, this later VO_2 phase does not exhibit the so attractive Mott reversible transition characteristics at T_c. The 3 phases mentioned above are known as VO_2 (T) for the tetragonal type, VO_2 (M_1) for the monoclinic type with the Mott phase transition, and VO_2 (M_2) for the non-transiting monoclinic type. Above the transition temperature T_c, VO_2 (T) adopts the tetragonal rutile (P42 /mnm) structure with chains of edge-shared VO_6 octahedral along the c-axis; the V–V distances along the chain are 0.2851 nm (Figure 5). Below T_C, i.e. in the monoclinic (P21/c)

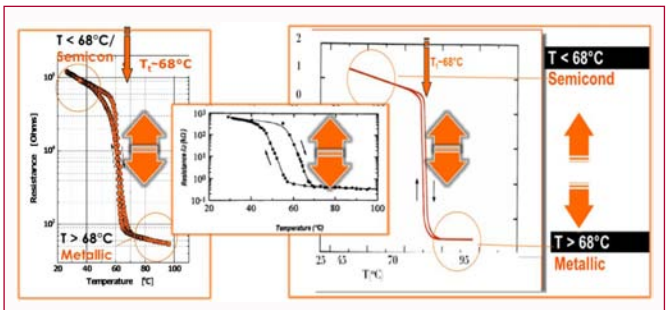

Figure 4: Tunable & reversible variation of the electric resistance of VO_2 in its form as (a) PLD crystalline thin film, (b) sol gel made thin film, and (d) bulk.

Table 1: Major characteristics of active phase of VO_2.

	VO_2 Insulating state (293.5K)	VO_2 Metallic state (> 342K)
Carrier mobility	0.1-1 cm^2/V·sec	1-10 cm^2/V·sec
Effective mass	1.6-7	1-3
Electron density	1019-1020 cm^{-3}	1-3x1021 cm^{-3}
Energy gap	0.6-0.7 eV	0

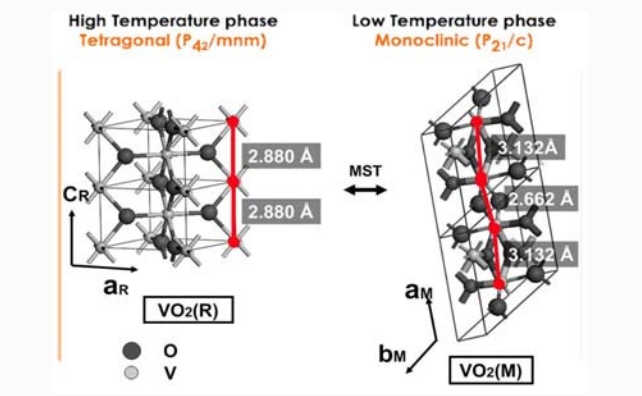

Figure 5: Tunable & reversible monoclinic (Low temperature)-rutile (High temperature) crystallographic phase transition of VO_2.

crystal structure of VO_2 (M_1), the dimerized vanadium atoms have alternate V–V distances of 0.2619 nm and 0.312 nm. It is widely accepted that the formation of an electron pair in the monoclinic crystalline structure results in the insulator phase while the tetragonal is metallic. The possible mechanism in relation to the phase transition may be due to changes in the 3d band structure associated with the crystal structure changes. As summarized in Figure 3, the upper d||—an unoccupied in conduction band of semiconductor phase is within the broad π*-band which is empty, but more strongly hybridized with oxygen 2p-orbitals and lies above the Fermi level E_F. In the metallic phase, however, all 3 d-bands are close to the Fermi-level. Above T_c, the main transitions are from occupied d||-valence band to unoccupied d||–π* mixed conduction band followed by resonant transitions to unoccupied excited states of the metallic phase. As a result the screening of the charge transfer by conduction electrons in metallic phase can take place by ultrafast laser excitation in addition to standard heating. The observed phase transition has been then associated with the optical interband transition in VO_2.

In view of the re-birth of the R&D global interest in the femtosecond governed optical and electronical singular properties of VO_2 coupled to the remarkable advances in ultrafast optical spectroscopy, this mini-review reports on the multifunctionality of smart nano-scaled VO_2 in optoelectronics & photonics; namely,

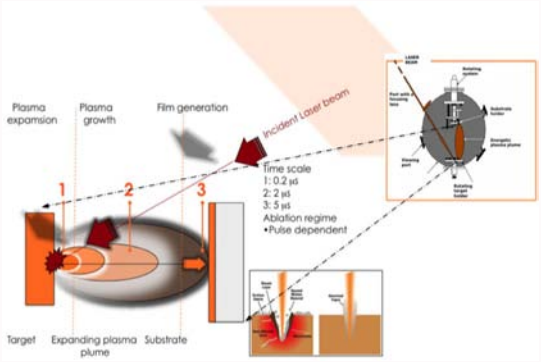

Figure 6: Typical standard Pulsed Laser Deposition (PLD) configuration ideal for the synthesis of highly crystalline VO_2 thin films.

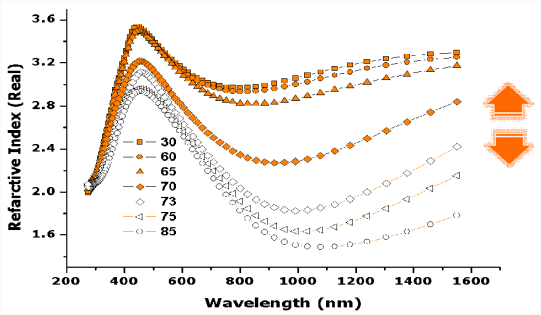

Figure 7: Room temperature variation of the conductometric sensing signal for the considered H_2 relative concentrations i.e. 140 ppm, 90 ppm, 50 ppm, and 14 ppm.

smart IR active coatings for solar energy heat management, ultrafast optoelectronics, tunable emissivity nanocoatings, tunable optical limiting, tunable nanoplasmonics, tunable femtosecond single optoelectronic nano-gating, and room temperature ultrasensitive gas sensing among others [12,14,15,18,24].

Experimental Results and Discussion

Pulsed laser deposition & synthesis of nano-scaled VO_2

As it is well established, high quality VO_2 nanostructures with physical/chemical characteristics close to bulk should exhibit a VO_2 (T) single phase component, a high degree of crystallinity in addition to the stringent stoichiometry O/V ratio of 2. In this regard, due to the ultimate non-thermodynamic equilibrium conditions, and yet with its handicap in terms of large homogeneous coatings, Pulsed Laser Deposition (PLD) was found as a sound solution to overcome these growth & stoichiometry problems relatively to the standard processes such as e-beam, evaporation, sol-gel, sputtering, chemical vapor deposition processes [28-30]. Indeed, in the case of the laser ablation, the target temperature at laser pulse peak can be as higher as 10^5 K i.e. 40eV with a local electric field E_{field} as intense as or even higher > 10^5 V/cm inducing a plasma which temperature is within the range of 3000 K-5000 K and ablated species with energy ranging from 1eV to 100 eV. As reported in the literature, specifically within the area of nanostructured binary, ternary or multi-oxides, PLD is by far a competitive synthesis methodology [31-33]. Furthermore, the PLD is conceptually and experimentally simple, yet highly versatile for nanostructured and multilayered systems. Its advantages for oxides and other chemically complex materials include stoichiometric transfer of the ablated material, growth from an energetic beam, high deposition rate, reactive deposition, and inherent simplicity for the growth of multilayered nano-structures [33]. Figure 6 shows the basic setup of a PLD whereby one can notice that the source of the plasma i.e. the laser source is decoupled from the vacuum chamber where the pressure can be varied from atmospheric to UHV. Likewise, a further major potential in the growth of nanostructures offered by the PLD is the possibility of achieving epitaxial growth at lower substrate temperatures due to the ultra-short time of laser-target interaction "≤ nanosec". In addition to minimizing undesirable interactions at the substrate-film interface, the PLD also enhances the possibility of producing compositionally homogeneous multi-component nanostructures under conditions that hinder decomposition into thermodynamically favored phases [31]. In the case of VO_2, the standard deposition conditions are generally as follows: a pressed powder pellet 1.5 cm in diameter and 2 mm thick with nominal composition VO_2 is used as a target. The target is mounted in a small vacuum system with a base pressure of 2.0×10^{-6} mbar, and irradiated through an excimer (generally KrF) laser source. A quartz lens is used to vary the energy density in the range of 0.5 J/cm^2-2.7 J/cm^2 on the target. The substrates are mounted at a distance of typically 25 mm from the pellet surface, close to the centre of the laser spot. The laser is fired at a repetition rate of 10 Hz with a number of shots depending on the film thickness. During deposition, the pressure in the vacuum chamber rises to about $1\text{-}2.5 \times 10^{-6}$ mbar [14,24].

Refractive index temperature modulation of nano-scaled VO_2

As it was mentioned previously, the MST phase transition in VO_2 causing a sharp change in the electronic resistivity over several orders of magnitude is directly related to the reversible closing/opening of the electrical/optical band gap. Hence, this transition is accompanied by a consequential and reversible variation of the dielectric constant and hence the refractive index, specifically in the infrared (IR) spectral range. This translates itself in VO_2 being optically IR mainly transparent and opaque in the semiconductor and metallic states respectively. Figure 7 depicts the thermal modulation of the real part of the refractive index n(λ,T) of a pulsed laser deposited ~ 400 nm coating of VO_2 onto quartz glass substrate derived from ellipsometry investigations [34]. As one can notice, these ellipsometry deduced results demonstrate plainly the significant modulation of the refractive index with temperature and its reversibility. More precisely, the depicted dispersion of n(λ,T) is reported at 6 different temperatures "T = 30°C, 60°C, 65°C, 70°C, 73°C, 75°C and 85°C"over a spectral range covering the UV-VIS and NIR, over 300 nm-1600 nm region. While the thermal dispersion of n(λ,T) is slightly sizeable in the UV-VIS range, it is substantially large in the NIR spectral part. At λ ~ 473nm for example, the refractive index changes from 3.52 to 2.91 while at about λ ~1000 nm, it diminishes significantly by nearly 50%. More precisely, it decreases from about 3.2 to 1.6 when the VO_2 coating is heated from 30°C to 85°C. Consequentially, such a significant and reversible thermal variation of the dispersion relation is of a special interest in the optical IR & Terahertz switching based devices in general and infrared modulation specifically. The following cases are among the likely potential optoelectronic technological applications of nanostructured VO_2.

Optical modulation in VO_2 nanostructures & solar heat regulation

The dispersion relation of Figure 7 and its tunability/reversibility are of a special importance for applications of nanostructured VO_2 in smart windows for solar heat regulation. Indeed, as reported in Figure 8, the IR radiation from the sun counts for about 52% of the solar

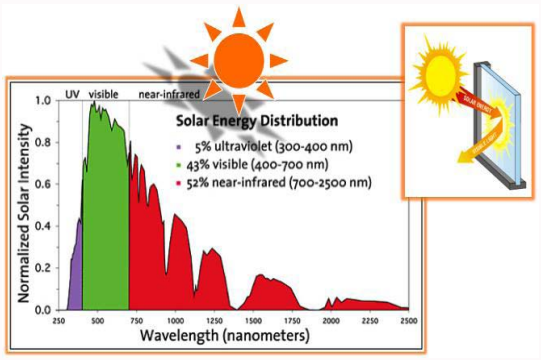

Figure 8: Spectral solar distribution at the earth level: ~5% UV (300 nm -400 nm), 43% VIS (400 nm-700 nm), and ~52% NIR (700 nm-2500 nm).

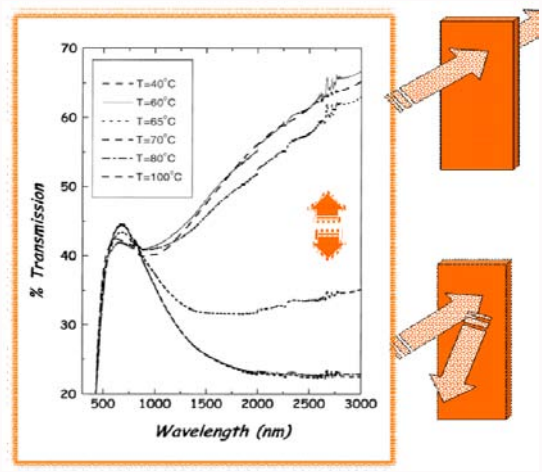

Figure 9: Normal incidence optical transmittance profiles of a pulsed laser deposited ~400 nm coating of VO_2 onto quartz glass substrate for six different temperatures; 40°C, 60°C, 65°C, 70°C, 80°C and 100°C.

intensity at the earth level. Hence, the heat management induced by the IR radiations from the sun using VO_2 coated windows would be ideal in minimizing the usage of standard air conditioning in building and automotives if the T_c can be as low as room temperature. As well established, such a T_c reduction can be induced by W or Mo doping. Figure 9 reports the optical transmittance of a pulsed laser deposited VO_2 coating onto glass substrate for six different temperatures; 40°C, 60°C, 65°C, 70°C, 80°C and 100°C" chosen so that they cover the optical response from IR transmittive state to IR opaque state to sun heat. As expected, the optical transmission exhibits a strong dependence with temperature in the infrared spectral region without a significant change in the visible region. At λ~3000 nm, the optical transmission is about 65% and 22% below and above the transition temperature of T_C~68°C. As it can be monitored, the average optical switching is smaller than 5% in the visible while in the NIR, it is larger than 35%. At 3000 nm, especially, the optical modulation is about ~55%. Consequentially, VO_2 could be used as a smart coating on glass windows to manage solar heat within the IR spectral range especially once doped with W which allows reducing T_c from ~68°C to closer to ~25°C. In addition to smart windows applications in the automotive and architectural-building industry, this sharpness of modulation from optically IR-transmitive to optically IR-reflective can be exploited for internal shutter devices applications in IR laser cavities or in fiber optics based devices. Certainly, as it was highlighted [34], these VO_2 based nano-photonics are adequate for close room-

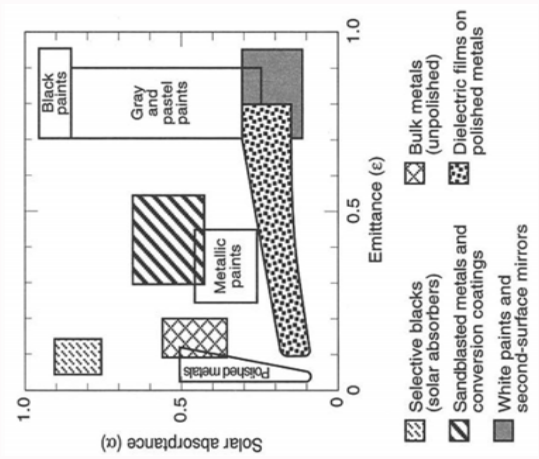

Figure 10: Solar absorptance (a)-Emissivity (e) diagram of standard materials and coatings.

temperature operation compatibility with fiber-optic environment, and high efficiency at telecommunication wavelengths "1.3 μm -1.5 μm". Moreover, it was demonstrated that the 300 mJ/cm² threshold for the photo-induced phase transition "which would be discussed in the following case study" is equivalent to a 150 pJ pulse for a typical 50 μm² mode size in a single-mode fiber, making such schemes attractive for real-world applications including the Terahertz regime.

Tunability of VO_2 nanostructures' emissivity & space applications

The thermal tunability of the spectral dispersion of the refractive index n(λ,T) of nanostructured VO_2 coatings as reported in Figure 6 is of a special interest in space applications. Indeed, in space environment and in particular for small satellites such as micro or/ and nano-satellites, VO_2 caotings can not only play a role of heat management related to the IR radiations from the sun but also a tunable emitter ensuring an optimal heat radiator behavior with a unique tunable emissivity configuration. This later characteristic is singular relatively to classical radiators governed by the standard Stefan's law. Figure 10 shows the solar absorptance (α)/emissivity (ε) diagram of major materials: (i) Solar blacks i.e. solar absorbers, (ii) sand lasted metals & conversion coatings, (iii) white paints & second-surface mirrors, (iv) unpolished bulk metals, and (v) dielectric films on polished metallic surfaces. As one can notice, excluding the last class of materials i.e. dielectric coatings, the emissivity cannot be varied over a large emissivity range. Likewise, even for the dielectrics, the highlighted zone in the (α)/(ε) diagram is related to a class of various coatings. In this section, it is intended to highlight that VO_2 onto special type of metallic films could exhibit a tunable thermal emissivity over a large range. This is of an exclusive importance in spacecraft technology in view of its Smart Radiation Device (SRD) potential [35]. As correctly stated by Hendaoui et al., this is by far an attractive approach in regard of achieving the thermal management of the internal temperature of the spacecraft as its emissivity is actively adapted to the external temperature. On and above the active heat load management, the VO_2 films are by their nature thin films and hence are nearly massless including the fact that they are easily integrated as a coating on the satellite directly. In view of VO_2 as a SRD integrated component, an ideal behavior of an SRD would correspond to a low (ε_L) and high (ε_H) emissivities at low and high temperatures respectively so to dissipate any additional not required heat. Hence, the performance of an ideal SRD are characterized

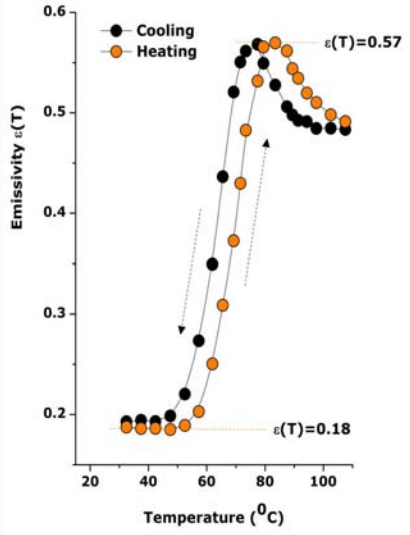

Figure 11: Reversible tunalbility of the emissivity positive-switching of an SRD VO_2 based coating consisting of a- Si:H/SiO_2/VO_2/Al foil substrate.

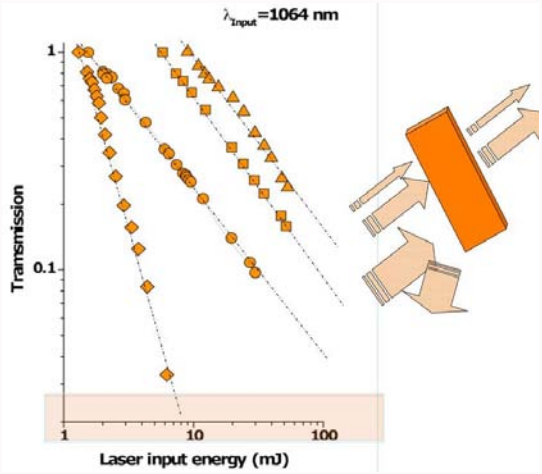

Figure 12: Log-Log Optical transmission/Laser input energy of 4 different pulsed laser deposited VO_2 nano-coatings onto quartz substrates with thicknesses of about ~64 nm, 109 nm, 400 nm and 1204 nm ±1nm. The experiments were carried out with a Nd-YAG laser source "l=1064 nm" beam impinging the samples in a normal incidence.

by the dynamic range of the emissivity $\Delta\varepsilon=(\varepsilon_H-\varepsilon_L)$; Higher is ε_H effective is the SRD. In other terms, and considering the Stefan equation of the thermal power emitted by a radiator of surface (S) at temperature (T) in half space $\Omega = \sigma\,\varepsilon\,S\,T^4$, higher ε_H values are suitable to achieve higher radiative exchange for smaller surfaces and weight (smaller satellites). In the case of VO_2, one can distinguish 2 cases. The first case for which the VO_2 is deposited on standard glass substrates whereby $\Delta\varepsilon=(\varepsilon_H-\varepsilon_L)$ is negative i.e. the so called negative emissivity-switching mode. The second case where VO_2 is deposited onto reflecting metallic substrates such as aluminium (Al) and hence allowing positive emissivity-stwitching $\Delta\varepsilon=(\varepsilon_H-\varepsilon_L) > 0$. It is this latter scenario which is of an interest in the heat management in nano-satellites in particular as demonstrated by Benkahoul et al. on optically polished Aluminium [36]. Because in this latter case, $\Delta\varepsilon=(\varepsilon_H-\varepsilon_L)$ was not large, Hendaoui et al. have succeeded to increase such a difference by boosting ε_H to higher values by adding a top layer of amorphous hydrogenated silicon a-Si:H onto oxidized silicon SiO_2 layer forming a λ/4 stack layer deposited on VO_2 layer itself coating an optically polished Aluminium substrate [37]. Within the current section, it is shown that this scheme can be extended to standard Aluminium sheets of 15.8×10^3 nm in thickness. Accordingly, a 263 ± 1nm of PLD deposited VO_2 onto clean standard Al sheet ($15.8\ 10^3$ nm in thickness) coated with an SiO_2 layer of 101 ± 1nm which in its turn coated with a hydrogenated amorphous silicon layer of 448 ± 1nm. This set of parameters have been inspired by the above mentioned Hendaoui et al's experiments. Figure 11 reports the normal incidence reflectivity of the a-Si:H/SiO_2/VO_2/Al sheet layered stack. As one can see the reflectivity, within the spectral 5 μm -25 μm range, at 25°C is higher than that at 97C which implies the targeted positive emissivity-stwitching $\Delta\varepsilon=(\varepsilon_H-\varepsilon_L)>0$. Indeed as derived from the reflectivity profiles and the dispersion relations n(λ,T) within the 5 μm -25 μm spectral range, the emissivity profile is temperature dependent and exhibits somehow the hysteresis behaviour during heating/cooling (Figure 11). This later thermal evolution mirrors the 1st order semiconductor-metallic phase transition of VO_2. The most important is that the minimum and maximum values of the emissivity are 0.18 (40°C) and 0.57 (83°C) respectively and hence allowing an emissivity-stwitching Δε of + 0.39. This relative variation $\Delta\varepsilon/\varepsilon_\Lambda$ which is about ~21.7% is adequate for developing VO_2 based SRD for active thermal control in small satellites and spacecrafts [34-36].

Optical limiting in VO_2 nanostructures & ultrafast laser protection

As it was mentioned in the introductory section, above the transition temperature T_c, VO_2 adopts the tetragonal rutile configuration with chains of edge-shared VO_6 octahedral along the c-axis where the V–V distances along the chain are 0.2851 nm. In the lower temperature monoclinic phase ($< T_C$), the dimerized vanadium atoms have alternate V–V distances of 0.2619 nm and 0.312 nm. As investigated by Semenov [37], this configuration is equivalent of those systems exhibiting 1 chain-like governed by Peierls model such as Platinum mixed valence complexes, $K_{0.3}Mo_3$ and $Rb_{0.3}MoO_3$ blue bronzes, TCNQ salts, TaS_3, $TaSe_3$, and NbS_3 [38]. Indeed, considering Semenov's investigations, the electronic spectrum of these compounds at the Fermi level has a quasi 1-D band formed when the wave functions of the d and f electrons of the neighbouring atoms arranged in the form of parallel chains overlap [37-40]. Within these Peierls governed chains of atoms like-systems, in the high-temperature metallic phase, the atoms are equidistantly located in the chain, whereas the conduction band of the electronic spectrum is half filled with electrons. When temperature reaches the critical value T_c upon cooling, the metallic phase becomes unstable and the metal–semiconductor phase transition MST occurs. This transition is characterized by the formation of a gap in the electronic spectrum of the system at the Fermi level and by pair-wise approach of atoms along the atomic chain [37-38] and hence the bandgap opening as schematically displayed by Figure 3. In this case, the atomic chain itself is deformed [41]. In addition, and as reported by Semenov once more [37], owing to the features of the electronic spectrum of the Peierls semiconductors characterized by the presence of Van Hove singularities [26], sharp [27] or smeared [28] edges of the gap, the photo-induced transitions from the semiconducting state to another state [27-29] are possible in a light field with a specially chosen central frequency of the optical spectrum and hence the photo-induced effects. More specifically, and near T_c, cavity-free optical bistabilities are observed in various Peierls systems with increasing absorption [30]. The dynamics of change in the structure of the crystal lattice and gap width in the electronic spectrum of such typical semiconductors

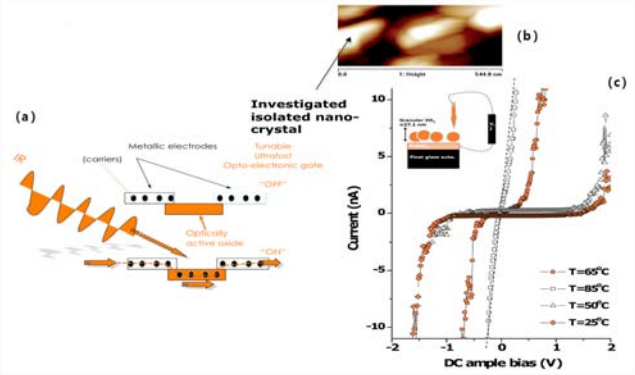

Figure 13: (a): Schematic view of the targeted tunable VO_2 based opto-electronic nanogate, (b) AFM imaging of the discontinuous VO_2 film cosnsting of generally non-percolating single VO_2 nanocrystals, and (c) Typical I-V curves on a single VO_2 nanocrystal at various temperatures: 298.5 K, 323.5 K, 338.5 K and 358.5K.

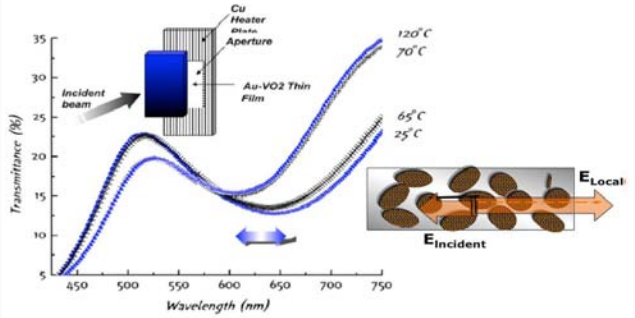

Figure 14: Normal incidence optical transmission of Au-VO_2 nanocomposites exhibiting a tunable plasma absorption within the range of 600nm -650 nm.

irradiated by the light field was investigated for various materials in several systems. Generally, it was observed that the new formed state is metallic [42]. In the case of VO_2, there are two alternative points of view on the cause of the formation of the semiconducting phase: electron–electron interaction usually considered in the Mott–Hubbard model [43] and the electron–phonon interaction (Peierls model) [44]. In regard of such models, the pioneering work of Semenov [40] is the early theoretical investigation to shed light on the photo-induced semiconductor to metal phase transition in VO_2 within the framework of a Peierls configuration. More specifically, the photo-induced effect consisting of the generation of non-equilibrium electron–hole pairs occuring owing to the electric dipole interaction of photons with the electronic sub-system of the semiconductor, was analyzed. The increase in this density caused by the electron–phonon interaction changes the crystal structure and electronic spectrum of the Peierls system. The dynamical equations were derived by Semenov for the order parameter of the metal–semiconductor phase transition as well as the kinetic equation for the density of non-equilibrium electron–hole pairs. In addition, an expression for the time τ of the photoinduced semiconductor–metal phase transition was derived from these equations in the case of ultrashort light pulses within the femtosecond regime fitting with the results of reported by Cavalleri et al. and Baum et al. [7-8]. It was shown that, to initiate optically the phase transition, the energy density Ø of the incident light pulse must be higher than a critical value $Ø_c$. Semenov has obtained quite interesting and convincing data in this regard for the VO_2 whose quasi-one-dimensional electron conduction band is formed owing to the overlapping of the 3d electron wavefunctions of vanadium atoms arranged in the form of chains parallel to the c crystal axis [24]. For temperatures below the critical value T_c~ 341K, the vanadium atoms in the chain pair-wise approach each other and an energy gap is formed at the Fermi level in the electronic spectrum [24]. Based on the physical values characteristic of VO_2 [24,40,41]: vanadium atom density of $N \approx 3 \times 10^{22}$ cm^{-3}, width of the d conduction band in the metallic phase of ≈ 1.1 eV, vanadium atom mass of ≈ 8.5×10^{-23} g, effective radius of the 3d atomic electron wave function R of ≈ 5×10^{-9} cm, refractive index in the semiconducting phase n_s ≈ 3.3, the distance between the top of the valence d band and the bottom of the conduction d band of the electronic spectrum in the semiconducting phase being ≈ 1.3 eV, the characteristic time of interband electron relaxation of = 3×10^{-11} s [45], the characteristic time of phonon relaxation at room temperature of ≈ 5×10^{-13} s [55], the matrix element of the dipole moment operator of ≈ 4×10^{-19} CGS units [47,48], and the optical reflection coefficient of the order of 20% [49]. For incident photons with the energy $h\nu_0$ = 1.6 eV (λ≈ 775 nm), the optical absorption coefficient γ_0 of ≈ 4×10^4 cm^{-1} and the critical energy density of the laser pulse, $Ø_c$ ≈ 18 mJ/cm^2, and derived by Semenov [40], the time of the phase transition induced by the laser pulse with the energy density Ø = 50 mJ/cm^2 is equal to $\tau \approx 50$ fs which is agreement with Cavalleri et al. and Baum et al. [7,8].

In addition to the standard induction of the semiconductor-metallic phase transition of VO_2 i.e by standard heating/cooling or pressure, the theoretical predictions of Semenov [40] and the experimental results of Cavalleri et al. [7] showed that that such MST transition can be a induced optically in a ultrafast manner. Hence nanostructured VO_2 coatings could exhibit femtosecond optical limiting response. Relatively to standard organic based materials, including porphyrins, phthalocyanines, fullerene (C_{60}), and carbon nanotubes (CNTs) liquid based suspensions which exhibit strong nonlinear extinction for high-intensity light, the VO_2 coatings are solid. Besides this solid state aspect of the VO_2 potential optical limiter samples, its advantage is correlated to the unique broad spectral modulation of VO_2 over all the NIR to the FIR spectrum. As shown in Figure 12, VO_2 nano-structured films exhibit indeed a singular optical limiting behavior. More accurately, the optical transmission of the 4 PLD deposited VO_2 nano-coatings onto quartz substrates with thicknesses of about ~64 nm, 109 nm, 400 nm and 1204 nm ±1nm exhibit a significant decrease of the optical transmission versus incident laser fluence. In this demonstrative case, the experiments were carried out with a Nd-YAG laser source "λ=1064 nm" beam impinging the samples in a normal incidence. The optical transmissions were measured versus the laser input energy within the range of 1 mJ to 90 mJ below the threshold damage of ~173 mJ; a value required to ignite the laser ablation of the VO_2 film coatings "in the current considered optical geometry". As depicted in Figure 12 reporting the Log-Log variation of the optical transmission versus the laser input energy, higher is the Nd-YAG input energy, smaller is the optical transmission for all VO_2 coatings. This is, indeed a crystal clear behavior of effective optical limiters. Such effectiveness seems to be thickness dependent. By extrapolation, at 1% transmission at 1064 nm, the threshold seems to be of about 8 mJ, 200 mJ, 580 mJ and 1070 mJ for the coatings of ~1204 nm, 400 nm, 109 nm and 64 nm respectively. Hence, one could, in the current case, conclude that the thickest VO_2 film of ~1204 nm seems to be the most suitable within the standard laser damage protection regulations. It can be expected that such VO_2 coatings would be ideal for high power laser CO_2 based

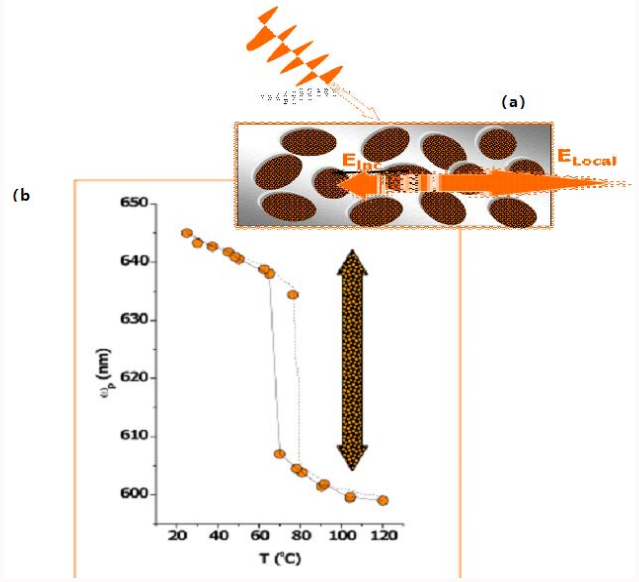

Figure 15: Evolution of the plasmon wavelength l_p of the Au-VO_2 nano-plasmonic, with the thermal cycling over the 25-120°C range. The reversible & tunable plasmon wavelength mirrors the 1st order phase transition of the VO_2 host matrix.

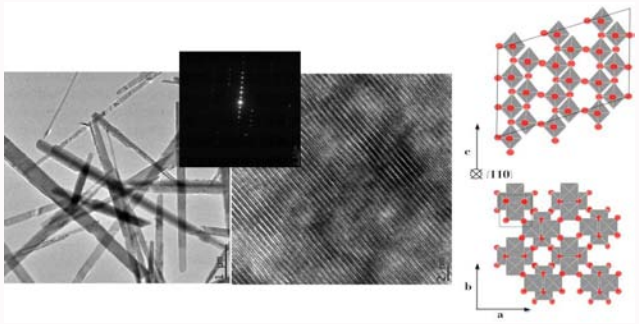

Figure 16: Typical electron transmission microscopy and electron diffraction pattern of the optimized synthesized powder of VO_2 (A) nanobelts with its corresponding crystallographic structure.

lasers sources as well as the tunable femtosecond sources which are mainly in the NIR range [12].

Optoelectronic tunability of VO_2 nanostructures: Optically controlled ultrafast e-gating

While extensive studies were conducted on VO_2 in terms of synthesis and investigations of its physical properties as well as its potential optoelectronic technological applications, very limited studies were performed on the variation of its electronic bandgap $E_g(T)$ in its nano-structured form [47-59]. For our best knowledge, and relatively to the published literature including the recent work of Yin et al. [6], this section reports on the experimental results of the thermal variation of the $E_g(T)$ of a single VO_2 nanocrystal and the validation of the possibility to engineer ultrafast and tunable VO_2 based opto-electronic nano-gates (Figure 13a) [60].

To perform the intended transport investigations in single nano-crystals of VO_2, it is necessary to engineer crystalline VO_2 films below the coalescence threshold i.e. consisting of spatially isolated nano-cystals of VO_2. PLD deposited VO_2 thin films onto conducting transparent oxide of F:SnO coated quartz substrates with thicknesses of ~27 nm ± 5 nm, 64 nm, 151 nm, 409 nm and 1218 nm ± 2 nm were prepared. This thickness range which was based on a previous study, was considered to obtain discontinuous and continuous films below and above the percolation threshold of the VO_2 nano-crystals. With the exception of the thinnest film (~27 nm ± 5 nm in thickness), the other samples (64 nm, 151 nm, 409 nm and 1218 nm ± 2 nm in thickness) showed almost identical surface morphology which indicates a continuous network of quasi-spherical nano-crystals with a polydisperse diameter distribution. The thinnest VO_2 film (~27 nm ± 5 nm) consists of quasi-isolated nano-crystals with an obloid-like shape anisotropy as shown in Figure 13b. The statistical scans provide average dimensions of ~469 ± 12 × 103 ± 9 × 29 ± 7 nm. More accurately, the average height value of ~29 nm ± 7 nm was obtained from additional statistical measurements over about 30 horizontally positioned VO_2 nanocrystals. One could notice that it is comparable to the average thickness of the thinnest film itself (i.e. 27 nm ± 5 nm) and hence could be considered as a discontinuous film of single grains. This thin film sample is used for the measurement of the temperature dependence of the I-V characteristics of individual/single VO_2 nano-crystals, and hence of the change in the band gap $E_g(T)$ through the MST transition as described below.

Figure 13c reports the measured I-V characteristics for a single isolated single nanocrystal of VO_2 in the thinnest discontinuous film of 27 nm ± 5 nm. The I-V profiles have been measured at 298.5 K, 323.5 K, 338.5 K and 358.5K. The used tunneling current was in the range of 0 nA-15 nA for an applied DC voltage varying from 0 V to 2.5V. As one notice, at $T < T_c$ (298.5, 323.5 and 338.5), the I-V characteristics exhibit a typical semiconductor behavior of the investigated isolated nano-crystal with the width of the "plateau" region being approximately equal as $2 \times E_g(T)$. Higher is the temperature; smaller is the bandagap which nearly closes that the vicinity of T_c. Indeed, at T= 358.5K the I-V characteristic is approximately linear, i.e. ohmic, pointing to a metallic behavior. Such a behavior of I-V thermal variation is reversible. From technological applications point of view, Figure 13c supports confidently the possibility of using such a device for ultrafast tunable opto-electronic gating as the MST/MIT reversible transition of the VO_2 nano-crystals can be induced optically in the femtosecond regime [61]. Likewise, such an applied aspect is being extended to engineer tunable ultrafast devices for surface enhanced Raman spectroscopy via bang gap engineering of core shell oxide/VO_2 nanostructures.

VO_2 for tunable ultrafast nano-plasmonics applications

Nano-composites with metallic nanoparticles embedded in an insulating host matrix as illustrated in Figure 10a, represent a specific class of nano-plasmonics with a distinctive plasmon resonance λ_p. As ω_p is proportional to $[n\ e^2/\varepsilon_0 m_{eff}\ ]/[1+2\varepsilon_{host}(\lambda)]$, one could anticipate its tunability via either the carrier density "n", the effective electronic mass "m_{eff}" of the metallic nano-particles, or through the dielectric function of the dielectric host matrix "$\varepsilon_{host}(\lambda)$". While the first two of these parameters can be varied by changing the nature of the nanoparticles, the third option requires a radical change in the host matrix. The latter is more effective, as it has been reported widely in the literature. Results with gold nanoparticles embedded in different host matrices including Fe_2O_3, SiO_2 , TiO_2 , and Nb_2O_5 have exhibited plasmon wavelength tunability via the variation of the refractive index of these different host matrices. The variation of λ_p is substantial: from 2.4eV to 1.7eV. Such a variation entails an explicit and a required host-matrix change. This is not a practical way to achieve plasmon wavelength tunability within the same nanodevice. The usage of VO_2 as a host matrix could be an elegant method for the

preparation of tunable and reversible nano-plasmonics where both the nature of the metallic nanoparticles and the host matrix remain fixed. This allows to thermally and reversibly tune λ_p in a controllable manner. This concurs with a consequential variation in the host material's optical constants. This reversible change in $n_{host}(\omega,T)$ i.e. $\varepsilon_{host}(\lambda,T)$ is pronounced in the infrared and hence for λ_p in the case of VO_2. To demonstrate the validity of this approach, a laser-deposited Au-VO_2 nano-plasmonics onto corning glass was investigated. The embedded Au nano-crystallites were ≈13nm in diameter. The optical transmission profiles at different temperatures indicated a clear variation of the plasma absorption as reported in Figure 14. The Au-VO_2 plasmon wavelength was about 648nm with the temperature below $T_c \approx 68°C$ "i.e. with the host matrix in its dielectric state, IR transmittive state". However, as the temperature increased past the transition point, changing the material into its metallic state, the wavelength shifted towards the blue "to ≈603nm". This sizeable variation of ≈45nm confirms the tunability of λ_p (T) through temperature change. In Figure 15, one can notice the evolution of the plasmon wavelength λ_p (T) of the Au-VO_2 nano-plasmonic, with the thermal cycling over the 25-120°C range: this result confirms undenialbly its thermal reversibility with a jump-like change. Such a sharp transition with a hysteresis of ≈16°C is inherent to the first order transition of the VO_2, which lasts less than 180fs [7-8,40]. One then can conclude that such an ultrafast temperature change in the refractive index should enable ultrafast nano-plasmonics with not only tunable plasmon wavelength $\lambda_p(T)$ but with tunable third order nonlinear optical susceptibility $\chi 3_{comp}(\lambda,T)$ as per described by Maaza et al. [15,18].

VO_2 nanobelts & room temperature H_2 gas sensing

In relation to hydrogen economy in general, and hydrogen gas sensing specifically, and in addition to standard nano-powders/thin films structures, extensive set of novel nano-scaled oxide materials such as nanowires, nanotubes, nanorods, and nanobelts based systems, are being investigated as ideal candidates for gas sensing applications. This is due to their set of singular surface characteristics, shape anisotropy and readiness for integrated devices [61-65]. This latter component includes their large surface/volume ratio, single crystalline structure due to their preferential growth, and great surface chemical active sites [66-67]. As reported in the literature, the 1-D nanostructures of well-established gas sensing materials such as SnO_2 [68-70], ZnO [71-72], In_2O_3 [73-74], and WO_3 [75-76] have shown higher sensitivity and selectivity, quicker response and faster time recovery, as well as an enhanced capability to detect gases at low concentrations compared with the corresponding thin film materials [87-78]. While the overall sensing characteristics of these so called 1-D nanomaterials are optimal, they are efficient at high temperature; generally above 200°C, resulting in a significant power consumption, in addition to device complexities in integration, which limits their technological applications. Consequentially, there is still a space and a need to develop 1-D nanomaterials for gas sensors that have very good sensing performance but at room-temperature. Unfortunately, for room temperature applications, there is a necessity to dope the above mentioned nano-scaled oxides with non-cost effective noble metals such as Pt, Pd, Au, Ru,….. Indeed, as demonstrated by Pearton et al. [79-80], ZnO nanorod sensors showed higher H_2 sensitivity and quicker response by sputter-depositing clusters of Pd or Pt onto the surface of the nanorods at room temperature compared with the undoped and the corresponding thin film sensors. Ramgir et al. [81] reported that 0.48% Ru-doped SnO_2 nanowires exhibited the highest sensitivity towards NO_2 gas at room temperature.

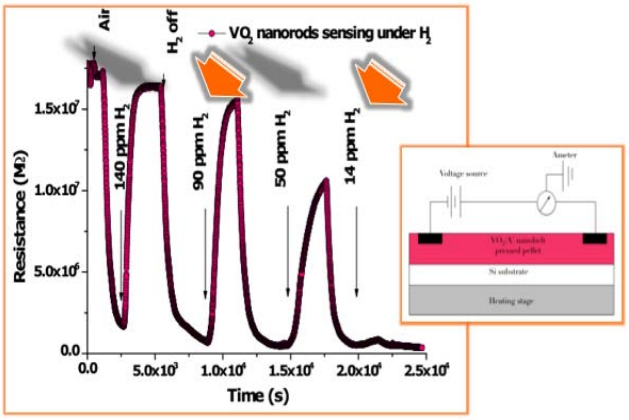

Figure 17: Room temperature variation of the conductometric sensing signal for the considered H_2 relative concentrations i.e. 140 ppm, 90 ppm, 50 ppm, and 14 ppm.

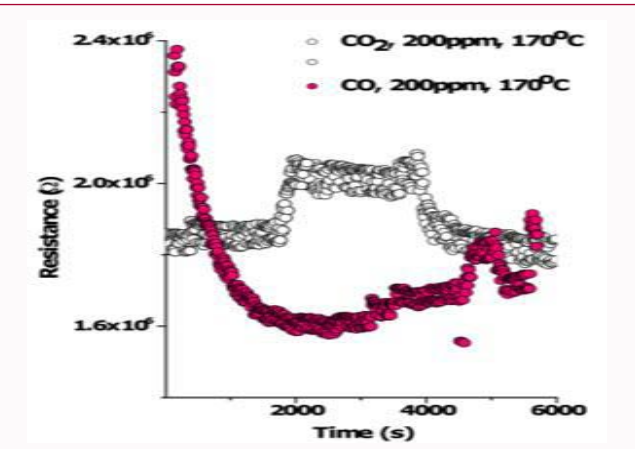

Figure 18: Minimum sensing parameters for both CO and CO_2 sensing of VO_2 (A) nanobelts: 200 ppm, T=170°C.

In this section and as reported by Simo et al. [82], it was shown for the first time that nanobelts of VO_2 exhibited room temperature enhanced hydrogen sensing properties (Figure 16). As highlighted below, the relatively large H_2 room temperature sensing in this Mott type specific oxide seems to have a limit below 0.17 ppm H_2. More precisely, and for the H_2 gas sensing experiments, a standard in-situ 2 contact points based system was used. The cold pressed VO_2(A) nanobelt pellet was squeezed between two Al electrodes and a Si substrate wafer while the whole was interfaced to a heating stage (25°C-300°C). The readings of the current and voltage during the heating and cooling stages were measured. The isothermal responses of the resistance of the pressed VO_2(A) nanobelts powder at different concentrations of H_2 fluxes were measured upon injection of H_2 balanced with N_2 as a gas carrier and refluxing with pure N_2. The reproducible experiments were conducted with different H_2 partial pressures equivalent to 140 ppm, 90 ppm, 50 ppm, 14 ppm and 0.17 ppm of H_2 carried by N_2. Before any H_2-N_2 experiment, the chamber was refluxed to minimize any contamination effect. Figure 17 reports a typical variation of the conductometric sensing signal for the above considered H_2 relative concentrations i.e. 140 ppm, 90 ppm, 50 ppm, 14 ppm and 0.17 ppm of H_2. The initial electrical resistance which is about $1.2 \times 10^7\ \Omega$ decreases to $0.18 \times 10^7\ \Omega$ upon initial refluxing.

Upon injection of 140 ppm H_2, it increases to reach a plateau-like. As in the case of effective sensing oxide based nano-systems, the electrical resistance decreases once H_2 gas flow is off. To estimate the H_2 detection limit, the room temperature conductometric measurements were performed at the various H_2 flow concentrations of 90 ppm, 50 ppm, 14 ppm and 0.17 ppm. It was noticed that the resistance variation which is reproducible with a small bar error, is still sensitive up to 0.17 ppm H_2. Compared to the various oxides as well as the 1-D reported nanosystems in the literature, this detection limit at room temperature is, indeed, significant [66-78] if not unique. Therefore, this detection limit is low enough for potential commercialization if the recovery and response times would be optimal. Concerning the response and the recovery time, the VO_2(A) nanobelts exhibit comparable values relatively to standard doped sensing nano-scaled oxides at room temperature and comparable H_2 concentration. More precisely, the average response times are ~840 seconds, ~890 seconds, ~1080 seconds, ~1020 seconds, and ~1050 seconds for 140 ppm, 90 ppm, 50 ppm, 14 ppm and 0.17 ppm of H_2 respectively. Likewise, the corresponding average recovery times are: ~455 seconds, ~870 seconds, ~1020 seconds, ~1037 seconds, and ~2080 seconds for 140 ppm, 90 ppm, 50 ppm, 14 ppm and 0.17 ppm of H_2 respectively. By comparison, the H_2 sensing of the equivalent oxide system i.e. ZnO nanorods, these latter possess a room temperature response time of the order of 600 seconds for 500ppm H_2. In addition to such a substantial characteristic, the sensitivity of the nanobelts S ($S=(R_{H2}-R_0)/R_0$, R_{H2} and R_0 are the sample resistance with and without H_2 gas respectively) is in the range of the values exhibited by standard 1-D oxides. In this case, the VO_2(A) nanobelts seem to present a better H_2 sensing sensitivity in the range of 90 ppm H_2 at room temperature. Finally, to shedlight on the sensing selectivity of the VO_2(A) nanobelts, further experiments were carried with other standard gases such as CO and CO_2. As the corresponding sensing characteristics seem to be very weak at room temperature under identical sensing conditions, threshold type experiments were conducted. Figure 18 shows one cycle conductometric sensor signal for CO and CO_2 gases. At it can be noticed, the sensing signal is at the background level yet at a temperature of 300°C and concentrations of 200 ppm CO and CO_2. Consequentially, it could be deduced that the VO_2(A) nanobelts seem to exhibit a noteworthy gas sensing selectivity towards H_2. In addition to the established applications of nano-scaled VO_2 [83-89], It is expected to witness a broad investigations of VO_2 in Memristors, Metamaterials and or Terahertz regime.

Conclusion

In this contribution, we reported on various functionalities of nano-structured VO_2. The tunability of the optical properties of VO_2 pulsed laser deposited based nano-strcutures under an external thermal stimuli. More specifically, and via the tunability of the refractive index in the IR spectral range, three cases were presented highlighting the singular photonics capabilities offered by VO_2 based nano-structures in the femtosecond regime. The three cases were: VO_2 as smart coating for solar heat regulation in smart windows, for optical limiting applications, and ultrafast tunable nano-plasmonics as well as novel tunable χ^3_{comp} NLO devices, in addition to room temperature H_2 selective gas sensing applications.

Acknowledgment

The author wishes to appreciate the financial support of the followings: the UNESCO UNISA Africa Chair in Nanosciences & Nanotechnology (U2ACN2), the South African Department. of Science & Technology, the National Research Foundation of South Africa, the University of South Africa, iThemba LABS-NRF, the African Laser Centre, the Abdus Salam ICTP-Trieste, the International Organization of Women in Science (OWSDW), the Academy of Science for the Developing World (TWAS), the Nanosciences African Network (NANOAFNET), and the French-South Africa bilateral cooperation programs. Likewise, the following colleagues are acknowledged: Prof. C. Sella, Prof. J. Lafait, Prof. A. Gibaud, Prof. I. Luk'yanchuk, Dr. J.B. Kana Kana, Dr. B.D. Ngom, Dr. A. Simo, Mr. M. Itani & Ms. L. Mathevula.

References

1. Morin FJ. Oxides Which Show a Metal-to-Insulator Transition at the Neel Temperature. Phys Rev Lett. 1959;3:34.
2. Mott NF. Metal-Insulator Transition. Rev Mod Phys. 1968;40:677.
3. Zylberstejn A, Mott NF. Metal-insulator transition in vanadium dioxide. Phys Rev B. 1975;11:4383.
4. Goodenough JB. Direct Cation--Cation Interactions in Several Oxides. Phys Rev. 1960;117:1442.
5. Hubbard J. Electron correlations in narrow energy bands. Procs R Soc. 1963;276: 38.
6. Adler D, Feinleib J, Brooks H, Paul W. Semiconductor-To-Metal Transitions in Transition-Metal Compounds. Phys Rev. 1967;155:851.
7. Cavalleri A, Dekorsy Th, Chong HHW, Schoenlein RW. Evidence for a structurally-driven insulator-to-metal transition in VO_2: A view from the ultrafast timescale. Phys Rev B. 2004;70:161102.
8. Baum P, Yang DS, Zewail AH. 4D visualization of transitional structures in phase transformations by electron diffraction. Science. 2007;318(5851):788-92.
9. Dal Conte S, Giannetti C, Coslovich G, Cilento F, Bossini D, Abebaw T, et al. Disentangling the electronic and phononic glue in a high-Tc superconductor. Science. 2012;335(6076):1600-3.
10. Parmigiani F. Ultrafast insulator-to-metal phase transition as a switch to measure the spectrogram of a supercontinuum light pulse. Appl Phys Lett. 2010;96:021102.
11. Lysenko S, Vikhnin V, Rua A, Fernandez F. Photoinduced Solid Phase Transformation in Vanadium Dioxide Films. Mater. Res Soc Symp Proc. 2006; 905E.
12. Maaza M, Hamidi D, Simo A, Chaudhary AK. Optical limiting in pulsed laser deposited VO_2 nanostructures. Optics Comms. 2012;285:1190.
13. Gal'perin VL, Khakhaev IA, Chudnovski FA, Shadrin EB. Zh.Tech.Phys. 1998; 43: 235.
14. Maaza M, Bouziane K, Maritz J. Direct production of thermochromic VO_2 thin film coatings by pulsed laser ablation. Optical Materials. 2000;15:41.
15. Maaza M, Ouassini N, Sella C, Beye AC. Optical limiting in pulsed laser deposited VO_2 nanostructures. Gold Bulletin. 2005;38:3.
16. Wang SB, Xiong BF, Zhou SB, Yi XJ. Preparation of 128 element of IR detector array based on vanadium oxide thin films obtained by ion beam sputtering. Sensors and Actuators A. 2005;117:110-114.
17. Balberbg I, Trokman S. High-contrast optical storage in VO_2 films. 1975;J Appl Phys 4:2111.
18. Maaza M, Sella C, Barak B, Ouassini N, Beye A. Thermal induced tunability of surface plasmon resonance in Au–VO_2 nano-photonics. Optics Comms. 2005;254:188.
19. Haverkort MW, Hu Z, Tanaka A, Reichelt W, Streltsov SV, Korotin MA, et al. Orbital-assisted metal-insulator transition in VO_2. Phys Rev Lett. 2005;95:196404.

20. Uhd JP, Fischer BM, Thoman A, Helm H, Suh JY, Lopez R, Haglund RF. Nanostructured gold films as broadband terahertz antireflection coatings. Phys Rev B. 2008;77: 195405.

21. Kübler C, Ehrke H, Huber R, Lopez R, Halabica A, Haglund RF Jr, et al. Coherent structural dynamics and electronic correlations during an ultrafast insulator-to-metal phase transition in VO_2. Phys Rev Lett. 2007;99:116401.

22. Liu M, Hwang HY, Tao H, Strikwerda AC, Fan K, Keiser GR, et al. Terahertz-field-induced insulator-to-metal transition in vanadium dioxide metamaterial. Nature. 2012;487:345-348.

23. Yin W, Wolf S, Ko C, Ramanathan S, Reinke P. Nanoscale probing of electronic band gap and topography of VO_2 thin film surfaces by scanning tunneling microscopy. J Appl Phys. 2011; 109:024311.

24. Maaza M, Hamidi D, Simo A, Kerdja T, Chaudhary AK. Optical limiting in pulsed laser deposited VO_2 nanostructures. Optics Comms. 2012; 285: 1190-1193.

25. Eyert V. The metal-insulator transition of NbO2: An embedded Peierls instability. EDP Sciences EPL (Europhysics Letters). 2002;58:851.

26. Goodenough JB (1971) Metallic Oxides. in Progress in Solid State Chemistry Ed. H Reiss, Pergamon press Oxford 5:145.

27. Cotell CM, Grabowski S. Novel Materials Applications of Pulsed Laser Deposition. MRS Bulletin. 1992;17: 44-53.

28. Shamm S, Scarel G, Fanciulli M. in "Rare earth oxide films", Eds. M. Fanciulli and G. Scarel. Appl Physics. 2007;106:153-77.

29. Schubert J, Heeg T, Wagner M, in "Rare earth oxide films", Eds. M. Fanciulli and G. Scarel, Topics Appl. Physics.2007; 106:115-26.

30. Lebedinskii Y, Zenkevitch A, Scarel G, Fanciulli M, in "Rare earth oxide films", Eds. M. Fanciulli and G. Scarel. Appl Physics. 2007;106:127-42.

31. Chrisey DB, Inam A. Pulsed Laser Deposition of High Tc Superconducting Thin Films for Electronic Device Applications. MRS Bulletin. 1992;17: 37.

32. Perriere J, Ranno L, Marechal C, Perez-Casero R, San Ramon RG, Martinez-Garcia D. Growth of Oxide Thin Films by Laser Ablation. In Laser Materials Processing: Industrial and Microelectronics Applications. 1994;2207:678-690.

33. Khamlich S, Ngom BD, Kotsedi CK, Bouziane K, Manikandan E, Maaza M. Morphological and Crystallographic Properties of Rare Earth Oxides Coatings Deposited by Double Dual Beam-Pld. Surf Rev Lett. 2014;21:1450001.

34. Kana JK, Ndjaka JM, Vignaud G, Gibaud A, Maaza M. Thermally Tunable Optical Constants of Vanadium Dioxide Thin Films Measured by Spectroscopic Ellipsometry. Optics Communications. 2011;28:807-12.

35. Hendaoui A, Émond N, Dorval S, Chaker M, Haddad E. Enhancement of The Positive Emittance-Switching Performance of Thermochromic VO_2 Films Deposited on Al Substrate for an Efficient Passive Thermal Control of Spacecrafts. Current Applied Physics. 2013;13:875-9.

36. Benkahoul M, Chaker M, Margot J, Haddad E, Kruzelecky R, Wong B, et al. Thermochromic VO_2 Film Deposited on Al with Tunable Thermal Emissivity for Space Applications. Solar Energy Materials and Solar Cells. 2011;95:3504-8.

37. Semenov al. Photoinduced Semiconductor-Metal Phase Transition in a Peierls System. Journal of Experimental and Theoretical Physics. 2007;104:68-75.

38. Minakova VE, Latyshev YI, Volkov VA. Nonlinear Conductivity Anomalies of the Quasi-One-Dimensional Compound m-TaS_3 near the Peierls Transition Temperature. JETP Letters. 1995;62:455-60.

39. L. N. Bulaevskioe , Usp. Fiz. Nauk 115 , 263 (1975) [Sov. Phys. Usp. 18, 131 (1975)].

40. Artemenko SN, Volkov AF, Zaitsev-Zotov SV. Quasi-One-Dimensional Conductors with a Charge Density Wave. Phys-Usp. 1996;39:403-7.

41. Eyert V. The metal-insulator transition of NbO2: An embedded Peierls instability. EDP Sciences EPL (Europhysics Letters). 2002;58:851.

42. Goodenough JB. Metallic Oxides, in Progress in Solid State Chemistry Ed. H Reiss, Pergamon press Oxford. 1971;5:145.

43. Rice TM, Launois H, Pouget JP. Comment on "VO_2: Peierls or Mott-Hubbard? A view from band theory" Phys Rev Lett. 1994;73:3042.

44. Wentzcovitch RM, Schulz WW, Allen PB. Wentzcovitch et al. reply. Phys Rev Lett. 1994;73:3043.

45. Belashenkov NR, Karasev VB, Solunin AA, Khakhaev IA, Tsibadze KS, Chudnovskii FA. Electron instabilities in the semiconducting phase of vanadium dioxide. Fiz Tverd Tela. 1994;36:2475-8.

46. Kittel C. Introduction to Solid State Physics , 7th edn. Wiley, New York, 1996; p. 236.

47. Andreev AV, Emel'yanov VI, Il'inskii YA. Cooperative Phenomena in Optics: Super radiance, Bistability. Phase Transitions. 1988:256.

48. Klyshko DN. Physical Fundamentals of Quantum Electronics. Russian edition, Moscow. 1986.

49. Cavalleri A, Dekorsy T, Chong HH, Kieffer JC, Schoenlein RW. Evidence for a structurally-driven insulator-to-metal transition in VO 2: A view from the ultrafast timescale. Physical Review B. 2004;70:161102.

50. Yin W, Wolf S, Ko C, Ramanathan S, Reinke P. Nano scale probing of electronic band gap and topography of VO 2 thin film surfaces by scanning tunneling microscopy. Journal of Applied Physics. 2011;109:024311.

51. Neuman CH, Lawson A. W, Brown R.F. Pressure Dependence of the Resistance of VO_2 J. Phys. Chem. 1964;41:1591.

52. Kosuge K. The phase transition in VO_2. Journal of the Physical Society of Japan. 1967;22:551-7.

53. Bongers PF. Anisotropy of the electrical conductivity of VO_2 single crystals. Solid State Communication. 1965;3:275-7.

54. Koide S, Takei H. Epitaxial growth of VO_2 single crystals and their anisotropic properties in electrical resistivities. Journal of the Physical Society of Japan. 1967;22:946-7.

55. Goodenough JB. Transition-metal oxides with metallic conductivity. Massachusetts Inst. of Tech., Lexington. 1965.

56. L. Ladd and W. Paul, Phys. Rev. Letts.17, 1286 (1966).

57. Adler D. Antiferromagnetism in Ti_2O_3. Physical Review Letters. 1966;17:139.

58. Sasaki H, Watanabe A. A new growing method for VO_2 single crystals. Journal of the Physical Society of Japan. 1964;19:1748.

59. Zylbersztejn A, Mott NF. Metal-insulator transition in vanadium dioxide. Phys Rev B. 1975;11:4383.

60. Maaza M, Simo A, Itani BM, Kana JK, El Harthi S, Bouziane K, et al. Phase transition in a single VO_2 nano-crystal: potential femtosecond tunable opto-electronic nano-gating. J Nanopart Res. 2014;16:2397.

61. Hernandez-Ramirez F1, Prades JD, Jimenez-Diaz R, Fischer T, Romano-Rodriguez A, Mathur S, et al. On the role of individual metal oxide nanowires in the scaling down of chemical sensors. Phys Chem Chem Phys. 2009;11:7105-10.

62. Yamazoe N. Toward innovations of gas sensor technology. Sensors and Actuators B. 2005;108:2-14.

63. Kiriakidis G, Moschovis K, Sadale SB. in " Sensors for environment , health and security", M.I. Baraton Editor, NATO Science for Peace and Security Series C: Environmental Security. 2009;I:159-178.

64. Kim WS, Kim HC, Hong SH. Gas sensing properties of MoO3 nanoparticles synthesized by solvothermal method. J Nanopart Res. 2010;12:1889-96.

65. Joshi RK, Kruis FE, Dmitrieva O. Gas sensing behavior of SnO1.8:Ag films composed of size-selected nanoparticles. J Nanopart Res. 2006; 8:797-808.

66. Pan ZW1, Dai ZR, Wang ZL. Nanobelts of semiconducting oxides. Science. 2001;291:1947-9.

67. Cui Y1, Lieber CM. Functional nanoscale electronic devices assembled using silicon nanowire building blocks. Science. 2001;291:851-3.

68. Comini E, Faglia G, Sberveglieri G, Calestani D, Zanotti L, Zha M. Tin oxide nanobelts electrical and sensing properties. Actuat. 2005; 2-6.

69. Comini E, Faglia G, Sberveglieri G, Pan ZW, Wang ZL, Stable and highly sensitive gas sensors based on semiconducting oxide nanobelts. Appl Phys Lett. 2002;81:1869-71.

70. Kolmakov A1, Klenov DO, Lilach Y, Stemmer S, Moskovits M. Enhanced gas sensing by individual SnO2 nanowires and nanobelts functionalized with Pd catalyst particles. Nano Lett. 2005;5:667-73.

71. Tien LC, Wang HT, Kang BS, Ren F, Sadik PW, Norton DP, et al. Room-temperature hydrogen-selective sensing using single Pt-coated ZnO nanowires at microwatt power levels. Electrochemical and Solid-State Letters. 2005;8:G230-2.

72. Lv Y, Guo L, Xu H, Chu X. Gas-sensing properties of well-crystalline ZnO nanorods grown by a simple route. Physica E: Low-dimensional Systems and Nanostructures. 2007;36:102-5.

73. Sberveglieri G, Baratto C, Comini E, Faglia G, Ferroni M, Ponzoni A, et al. Synthesis and characterization of semiconducting nanowires for gas sensing. Sensors and Actuators B: Chemical. 2007;121:208-13.

74. Wang CY, Ali M, Kups T, Röhlig CC, Cimalla V, Stauden T, et al. NO x sensing properties of In_2O_3 nanoparticles prepared by metal organic chemical vapor deposition. Sensors and Actuators B: Chemical. 2008;130:589-93.

75. Rout CS, Hegde M, Rao CN. H 2 S sensors based on tungsten oxide nanostructures. Sensors and Actuators B: Chemical. 2008;128:488-93.

76. Rout CS, Govindaraj A, Rao CN. High-sensitivity hydrocarbon sensors based on tungsten oxide nanowires. Journal of Materials Chemistry. 2006;16:3936-41.

77. Liu Z, Yamazaki T, Shen Y, Kikuta T, Nakatani N, Li Y. O_2 and CO sensing of Ga 2 O 3 multiple nanowire gas sensors. Sensors and Actuators B: Chemical. 2008;129:666-70.

78. Tien LC, Sadik PW, Norton DP, Voss LF, Pearton SJ, Wang HT, et al. Hydrogen sensing at room temperature with Pt-coated ZnO thin films and nanorods. Applied Physics Letters. 2005;87:222106.

79. Wang HT, Kang BS, Ren F, Tien LC, Sadik PW, Norton DP, et al. Hydrogen-selective sensing at room temperature with ZnO nanorods. Applied Physics Letters. 2005;86:243503.

80. Ramgir NS, Mulla IS, Vijayamohanan KP. A room temperature nitric oxide sensor actualized from Ru-doped SnO 2 nanowires. Sensors and Actuators B: Chemical. 2005;107:708-15.

81. Simo A, Mwakikunga B, Sone BT, Madjoe R, Maaza M. International Journal of Hydrogen Energy. 2014;39:8147-57.

82. Kana JB, Ndjaka JM, Ateba PO, Ngom BD, Manyala N, Nemraoui O, et al. Thermochromic VO_2 thin films synthesized by rf-inverted cylindrical magnetron sputtering. Appl Surf Sci 2008;254:3959-63.

83. J.B. Kana Kana, D.Knoesen, J.M. Ndjaka, O. Nemraoui, M. Maaza, Appl. Surf. Science 2009

84. Mwakikunga BW, Maaza M, Hillie KT, Maaza M. From phonon confinement to phonon splitting in flat single nanostructures: A case of VO_2@V2O5 core–shell nano-ribbons. Vibrational Spectroscopy. 2012;61:105-111.

85. Kana JBK, Ngom BD, Maaza M. Active modulation of the optical absorption coefficient of sputtered VO_2 nanostructure by external temperature stimuli. J Optics 2014, 43:28-33.

86. Madida IG, Simo A, Sone B, Maity A, Kana JB, Gibaud A, et al. Submicronic VO_2–PVP composites coatings for smart windows applications and solar heat management. Solar Energy. 2014;107:758-69.

87. Mathevula L, Ngom BD, Kotsedi L, Sechogela P, Doyle TB, Ghouti M, et al. Thermochromic VO_2 on Zinnwaldite Mica by pulsed laser deposition. App Surf Sci. 2014;314:476-80.

88. Diallo A, Ngom BD, Maaza M. Effect of substrate temperature on the structure and the metal insulator transition in pulsed laser deposed V02\ films on soda lime glass. J Optics. 2015;44:36-44.

89. Abdellaoui I, Merad G, Maaza M, Abdelkader HS. Electronic and optical properties of Mg-, F-doped and Mg-F-codoped M1-VO_2 via hybrid density functional calculations. J All Comp. 2016;658: 569-75.

90. Madiba IG, Emond N, Chaker M, Thema FT, Tadadjeu SI, Muller U, et al. Effects of gamma irradiations on reactive pulsed laser deposited vanadium dioxide thin films. App Surf Sci. 2017;411:271-8.